Author/s:
Ju, Y;Kelly, HG;Dagley, LF;Reynaldi, A;Schlub, TE;Spall, SK;Bell, CA;Cui, J;Mitchell, AJ;Lin, Z;Wheatley, AK;Thurecht, KJ;Davenport, MP;Webb, AI;Caruso, F;Kent, SJ

Title:
Person-specific biomolecular coronas modulate nanoparticle interactions with immune cells in human blood

Date:
2020-11-24

Citation:
Ju, Y., Kelly, H. G., Dagley, L. F., Reynaldi, A., Schlub, T. E., Spall, S. K., Bell, C. A., Cui, J., Mitchell, A. J., Lin, Z., Wheatley, A. K., Thurecht, K. J., Davenport, M. P., Webb, A. I., Caruso, F. & Kent, S. J. (2020). Person-specific biomolecular coronas modulate nanoparticle interactions with immune cells in human blood. ACS Nano, 14 (11), pp.15723-15737. https://doi.org/10.1021/acsnano.0c06679.

Persistent Link:
https://hdl.handle.net/11343/249849

Person-Specific Biomolecular Coronas Modulate Nanoparticle Interactions with Immune Cells in Human Blood

Yi Ju,[1] Hannah G. Kelly,[2] Laura F. Dagley,[3,4] Arnold Reynaldi,[5] Timothy E. Schlub,[6] Sukhdeep K. Spall,[3,4] Craig A. Bell,[7] Jiwei Cui,[1,8] Andrew J. Mitchell,[9] Zhixing Lin,[1] Adam K. Wheatley,[2] Kristofer J. Thurecht,[7] Miles P. Davenport,[5] Andrew I. Webb,[3,4] Frank Caruso,[,1] and Stephen J. Kent*[,2]*

[1]ARC Centre of Excellence in Convergent Bio-Nano Science and Technology, and the Department of Chemical Engineering, The University of Melbourne, Parkville, Victoria 3010, Australia

[2]ARC Centre of Excellence in Convergent Bio-Nano Science and Technology, Department of Microbiology and Immunology, Peter Doherty Institute for Infection and Immunity, The University of Melbourne, Parkville, Victoria 3010, Australia

[3]The Walter and Eliza Hall Institute of Medical Research, 1G Royal Parade, Parkville, Victoria 3052, Australia

[4]Department of Medical Biology, The University of Melbourne, Parkville, Victoria 3010, Australia

[5]Infection Analytics Program, Kirby Institute for Infection and Immunity, University of New South Wales Australia, Sydney, New South Wales 2052, Australia

[6]Sydney School of Public Health, Faculty of Medicine and Health, The University of Sydney, Sydney, New South Wales 2006, Australia

[7]ARC Centre of Excellence in Convergent Bio-Nano Science and Technology, Centre for Advanced Imaging, Australian Institute for Bioengineering and Nanotechnology, ARC Training Centre for Innovation in Biomedical Imaging Technology, The University of Queensland, St. Lucia, Queensland 4072, Australia

[8]Key Laboratory of Colloid and Interface Chemistry of the Ministry of Education, School of Chemistry and Chemical Engineering, Shandong University, Jinan, Shandong 250100, China

[9]Department of Chemical Engineering, Materials Characterisation and Fabrication Platform, The University of Melbourne, Parkville, Victoria 3010, Australia

ABSTRACT

When nanoparticles interact with human blood, a multitude of plasma components adsorb onto the surface of the nanoparticles, forming a biomolecular corona. Corona composition is known to be influenced by the chemical composition of nanoparticles. In contrast, the possible effects of variations in the human blood proteome between healthy individuals on the formation of the corona and its subsequent interactions with immune cells in blood are unknown. Herein, we prepared and examined a matrix of 11 particles (including organic and inorganic particles of 3 sizes and 5 surface chemistries) and plasma samples from 23 healthy donors to form donor-specific

biomolecular coronas (personalized coronas) and investigated the impact of the personalized coronas on particle interactions with immune cells in human blood. Among the particles examined, poly(ethylene glycol) (PEG)-coated mesoporous silica (MS) particles, irrespective of particle size (800, 450, or 100 nm in diameter), displayed the widest range (up to 60-fold difference) of donor-dependent variance in immune cell association. In contrast, PEG particles (after MS core removal) of 860, 518, or 133 nm in diameter displayed consistent stealth behavior (negligible cell association), irrespective of plasma donor. For comparison, clinically relevant PEGylated doxorubicin-encapsulated liposomes (Doxil) (74 nm in diameter) showed significant variance in association with monocytes and B cells across all plasma donors studied. An in-depth proteomic analysis of each biomolecular corona studied was performed and the results were compared against the nanoparticle–blood cell association results, with individual variance in the proteome driving differential association with specific immune cell types. We identified key immunoglobulin and complement proteins that explicitly enriched or depleted within the corona and which strongly correlated with the cell association pattern observed across the 23 donors. This study demonstrates how plasma variance in healthy individuals significantly influences the blood immune cell interactions of nanoparticles.

KEYWORDS personalized protein corona, human blood assay, particle–immune cell interactions, proteomics analysis, immunoglobulin, complement proteins

Nanoengineered particles hold promise for developing the next generation of therapeutics.[1] However, only a limited number of nanoparticles have demonstrated successful clinical outcomes.[2] A potential confounding factor for the use of nanoparticles in biomedical applications is recognition and inactivation by the immune system. When synthetic or engineered nanoparticles are introduced into the blood, they are coated with a multitude of host-derived biological

components (including proteins, carbohydrates, and lipids) within the bloodstream.[3–6] These (biological component) coatings on the surface of the nanoparticles make up the biomolecular corona and alter the size and surface composition of the nanoparticles, giving them a biological identity that is distinct from their synthetic identity.[7–9] Recently, the formation of biomolecular coronas *in vivo* on nanoparticles in human systemic circulation was described.[10] Importantly, the biomolecular corona guides interactions with immune cells in the blood,[11] which consequently modulates the fate and/or utility of a given nanoparticle.[12]

The human plasma proteome varies significantly depending on the genetic background, lifestyle, and underlying health conditions of an individual.[13] The biomolecular corona formation is also likely to be donor-specific or personalized.[14] This phenomenon has been observed on graphene oxide where the composition of the corona is strongly influenced by the patient's specific disease.[15] A recent study has shown that complement protein C1q is abundant in the biomolecular corona formed in the serum of patients with lung cancer, which leads to the activation of macrophages and elevated pro-inflammatory cytokine production.[16] Furthermore, the molecular fingerprint offered by a personalized corona has been studied as a diagnostic tool for early disease detection.[17–19] Research on personalized coronas of nanoparticles has focused on disease-derived plasma variance although it is largely unclear if the corona variance is due to disease or to normal human variance.[15,16,20,21] Given the outbred nature of humans, we hypothesize that individual protein coronas, even in healthy subjects, could vary substantially and influence nanoparticle interaction with human blood cells. Healthy volunteers are commonly studied in early-stage clinical trials to provide information on safety and pharmacokinetics of new drug formulations.[22] Unravelling the effects of blood variance among healthy donors on the corona composition and immune

recognition of nanoparticles could lead to rational improvements of nanoparticle-based medicines and ultimately enhance their clinical utility.

Poly(ethylene glycol) (PEG), an FDA-approved polymer that enhances surface hydrophilicity, is a prototypic "low-fouling" material that reduces association and uptake by immune cells.[23] This makes PEG-based particles a widely used drug delivery platform to avoid clearance by phagocytic cells.[24] For example, PEGylated doxorubicin-encapsulated liposomes were approved by the FDA in 1995 as a nanoscale anticancer agent (Doxil) owing to its substantial reduction in cardiotoxicity.[25] Using mesoporous silica (MS) replication, we have previously engineered PEG particles with precisely controlled size (from 150 nm to 1.4 μm), structure (presence or absence of MS cores), stiffness (0.3 to 3 mN m^{-1}; similar to red blood cells) and surface chemistry (functionalized with various targeting ligands such as antibodies and peptides).[26–28] Our preliminary reports demonstrated that the recognition and sequestration of PEG particles by blood leukocytes strongly influenced their biological utility, including biodistribution, circulation time, and tumor targeting *in vivo*.[27,29,30] However, the composition of the biomolecular corona on PEG-based nanoparticles in complex biological systems and how this influences particle–immune cell interactions remain unexplored.

Herein, we prepared MS particles, PEGylated MS (PEG-MS) particles, and PEG particles (where the MS template is removed) with different sizes (800, 450, 100 nm) and investigated the impact of a personalized biomolecular corona upon interactions with peripheral blood mononuclear cells (PBMCs). Importantly, we found that the personalized coronas formed on the PEG-MS nanoparticles from plasma of each donor significantly influenced their interactions with monocytes and B cells. These findings were independent of particle size, dosage, or source of PBMCs (from which individual donors). This phenomenon was further explored by forming

personalized coronas from the plasma of 23 healthy donors on nanoparticles with distinct physicochemical properties (including MS, PEG-MS, PEG, Doxil, and polystyrene (PS) nanoparticles). PEG-MS and Doxil nanoparticles showed high variability in immune cell association when coated with coronas from different individuals. The compositions of the personalized coronas formed on the PEG-MS nanoparticles from 23 donors were further characterized by mass spectrometry-based proteomics. Distinct proteomic fingerprints were observed on the donor-specific coronas, and the abundance of particular plasma proteins strongly correlated with nanoparticle association with specific immune cells. Immunoglobulin and complement proteins were identified as the key proteins enriched explicitly on the nanoparticles that correlated with enhanced immune cell association. We note that although these key proteins are not present as one of the most abundant proteins in the corona or in neat plasma, they play a key role in regulating immune recognition, thus highlighting the "quality" over "quantity" effect in corona composition with respect to immune cell association.

RESULTS AND DISCUSSION

Synthesis and Characterization of MS, PEG-MS, and PEG Particles. MS particles with an average size of 800, 450, and 100 nm (denoted as MS-800, MS-450, and MS-100, respectively) were synthesized using a surfactant templating method.[31,32] The spherical morphology and porous structure of MS particles were observed from the transmission electron microscopy (TEM) images in Figure 1A. PEG-MS and PEG particles were prepared *via* the MS templating method as previously described.[27] Briefly, PEG-MS particles were synthesized by infiltrating 8-arm-PEG-NH_2 into MS particles, followed by cross-linking with 8-arm-PEG succinimidyl succinate (8-arm-PEG-NHS). After removing the MS particles, spherical PEG particles were obtained (Figure 1A). MS, PEG-MS, and PEG particles were fluorescently labeled by covalent conjugation of *N*-

hydroxysuccinimide (NHS)-activated Alexa Fluor dye (AF488 or AF647). PEG-MS and PEG particles templated from MS-800, MS-450, and MS-100 are denoted as PEG-MS-800, PEG-MS-450, and PEG-MS-100, and PEG-800, PEG-450, and PEG-100, respectively. Fluorescence microscopy and dynamic light scattering (DLS) analyses revealed the colloidal stability of MS, PEG-MS, and PEG particles in human plasma (Figure 1B, C and Figure S1). Regardless of particle size, all three particle systems were well dispersed without aggregation after incubation for 1 h in human plasma at 37 °C. The diameter of the MS, PEG-MS, and PEG particles changed negligibly in the presence of a biomolecular corona (Figure 1D).

Human Blood Immune Cell Assay to Study the Influence of the Corona. The sequestration of nanoparticles by circulating leukocytes and the reticuloendothelial system leads to their rapid removal from the bloodstream, a major obstacle associated with drug delivery carriers.[33] Nanoparticle interactions with cells are commonly studied using immortalized cell lines but these poorly mimic the complex *in vivo* environment.[34] Here, we modified a previously developed human blood assay[35] to explore the effect of the biomolecular corona on cellular interactions with primary immune cells. Plasma and PBMCs (including lymphocytes and monocytes) were separated from fresh human blood of a healthy donor (Scheme 1). The particles (MS, PEG-MS, PEG) were preincubated with plasma to facilitate the formation of a biomolecular corona, then incubated with washed PBMCs in serum-free media for 1 h at 37 °C. To minimize the influence of any particle sedimentation,[36] particle and cell suspensions were mixed by gentle vortexing every 20 min during incubation. Cells were subsequently labeled with fluorescent antibody cocktails and analyzed by flow cytometry to identify specific cell types associating with particles (Figure S2). In the absence of a plasma corona, MS particles have significantly higher cell association with phagocytic cells (monocytes) and B cells compared with PEG-MS and PEG particles (Figure 2A–

C), driven by the surface chemistry of particles, as previously reported.[11] In the presence of a plasma corona, only the MS and PEG-MS particles associated with monocytes and B cells (Figure 2A–C) and particle association with T cells and NK cells were low (Figure S4), consistent with our previous observations.[11,27] Compared to the MS particles, the PEG-MS particles displayed a more distinct difference in cell association between the absence of a corona, "no corona", and the presence of a corona, "with corona". The presence of a plasma biomolecular corona was a prerequisite for particle association with both monocytes and B cells to occur. This difference was more prominent as the particle size decreased (Figure 2A–C). Cross-sectional images of the monocytes and B cells sorted from PBMCs (Figure 2D–F) showed that the MS and PEG-MS particles were likely internalized by monocytes, whereas the particles were exclusively bound on the cell membrane of B cells.

Association of Particles with Immune Cells is Dependent on Plasma. The physiological microenvironment of nanoparticles is an important consideration in the formation and effects of biomolecular coronas. Personalized coronas were formed after incubating nanoparticles with human blood plasma from healthy donors who are expected to exhibit different plasma proteomes. We used plasma from two healthy donors to form the personalized biomolecular corona on a matrix of nine particles of different size and composition. Particles were subsequently incubated with washed PBMCs (from one of the healthy donors) in serum-free media to allow comparison between different plasma coronas (Figure 3A). Changing the plasma source from donor 1 to donor 2 led to different particle association behaviors (in terms of cell association percentage) with monocytes and B cells, with the most distinct difference observed for MS-100 and PEG-MS-100 nanoparticles (Figure 3B–D). Notably, PEG-MS-100 nanoparticles with a biomolecular corona from plasma donor 1 (corona donor 1) associated with more than 80% of monocytes and B cells,

whereas the same particle type with corona donor 2 displayed less than 4% cell association, similar to the result obtained in the absence of a corona ("No corona") (Figure 3D). All six MS and PEG-MS particles, irrespective of particle size, displayed higher particle signals on monocytes and B cells when the corona from donor 1 was used than that from donor 2 (Figure 3E–G). In comparison, PEG particles displayed consistent stealth behavior with minimal binding to monocytes and B cells, irrespective of plasma donor.

The difference in cell association between the two corona donors was further examined at different particle dosages. The median fluorescence intensity (MFI) of cells was used to quantify cell association. In agreement with the results discussed earlier, MS and PEG-MS particles with corona donor 1 showed consistently higher cell association with monocytes and B cells compared with the same particles with corona donor 2 (Figure S6A–C) at all dosages examined. However, depending on the particle dosage, an approximately 2–10-fold difference in MFI was observed between corona donor 1 and donor 2 for MS-800, MS-450, MS-100, PEG-MS-800, and PEG-MS-450 particles (Figure S7). Notably, PEG-MS-100 nanoparticles displayed the most significant difference between the two corona donors, displaying up to an approximately 60-fold change in MFI for both monocytes and B cells.

Impact of Personalized Corona Is Independent of Cell Donors. Changing the plasma source from one healthy donor to a different healthy donor significantly influenced particle–immune cell association. To determine whether this impact was primarily due to the plasma corona or the immune cells of the donor (allogeneic *versus* autologous PBMCs), we prepared separate sets of plasma and PBMCs from donor 1 and donor 2 and performed a cross-over experiment (Figure S8). PEG-MS-100 nanoparticles were pre-incubated with the plasma from donor 1 or 2 to form personalized coronas before adding to washed PBMCs from each donor. Varying the donor of the

PBMCs had minimal impact on cell association, with the association rates being driven primarily by the plasma corona of a given individual on the particles (Figure 4, Figure S10). Irrespective of the PBMC donor, the particles with corona donor 1 displayed a consistently higher cell association with monocytes (16- and 46-fold change for cell association percentage and MFI, respectively) and B cells (3- and 7-fold change for cell association percentage and MFI, respectively) compared with the same particles with corona donor 2.

Personalized Biomolecular Corona Dictates the Degree of Cell association. Using plasma from two healthy donors, we observed that a personalized biomolecular corona modulated particle–immune cell association in a donor-specific manner. Next, we examined the generalizability of this finding using plasma from a larger number of healthy donors and a broader range of nanoparticles (see characterization details in Table S1), *i.e.*, MS-100, PEG-MS-100, PEG-100, 100 nm polystyrene (PS-100) nanoparticles, and PEGylated doxorubicin-encapsulated liposomes that contain the same lipid composition and drug/lipid ratio as clinically used liposomal doxorubicin agent (Doxil). Plasma from 23 healthy donors was used to form personalized biomolecular coronas around each nanoparticle. Among the five nanoparticles studied, MS-100, PEG-MS-100 and Doxil particles exhibited the most significant variance in association with monocytes and B cells across plasma from 23 donors (Figure 5). To facilitate visual comparison between different particles, donors 3 to 23 are numbered based on PEG-MS-100 particle association with monocytes (from high to low). Spearman correlation analysis revealed that the cell association patterns of MS-100, PEG-MS-100, and Doxil are different from each other; however, the monocyte and B cell association is highly correlated for a given particle type (Figure S11). This highlights that the synthetic nature of nanoparticles plays a vital role in the formation

and effect of personalized coronas and suggests that the monocyte and B cell associations may be regulated by the same proteins within the corona.

In contrast, the cell association of PEG-100 and PS-100 nanoparticles was not influenced by a personalized biomolecular corona (Figure 5E–H). PEG-100 exhibited consistently minimal cell association irrespective of plasma donor. As reported in our previous study, the thickness of these PEG particles after air drying is about 1/100 of the diameter, indicating that they are highly hydrated in aqueous solution, thereby leading to minimal association with leukocytes.[27] PS-100 nanoparticles consistently displayed high association with monocytes and to a lesser degree with B cells, which is likely due to their well-described high fouling (hydrophobic) surface, leading to nonspecific adsorption of plasma proteins.[37] In addition, PS particles have been shown to efficiently bind bovine serum albumin (BSA) that denatures upon adsorption, leading to binding to scavenger receptors on cell surfaces.[38] It is possible that human serum albumin may be abundant in the coronas of PS-100 particles, resulting in reduced variations in cell association.

Personalized Biomolecular Corona Displayed Distinct Proteomic Fingerprints. To understand the influence of personalized corona on particle–immune cell interactions, we investigated the composition of biomolecular coronas formed on PEG-MS-100 nanoparticles using mass spectrometry-based proteomics. PEG-MS-100 nanoparticles were selected as they demonstrated significant corona donor-dependent variance in cell association with immune cells and could withstand multiple centrifugation steps required during sample preparation for the proteomics study. Three technical replicates from each personalized corona formed on PEG-MS-100 nanoparticles were analyzed, with neat plasma samples as reference. Relative protein abundance changes were quantified using the normalized label-free quantification (LFQ) intensities, which were calculated using the MaxLFQ algorithm in MaxQuant.[39]

This proteomic analysis identified a median of 406 (range of 240–730) proteins from personalized coronas of PEG-MS-100 nanoparticles (Figure S12), while a median of 311 (range of 281–356) proteins were identified from neat plasma across the corresponding 23 healthy human donors (Figure S13). The total relative protein abundance of corona proteins identified in the personalized coronas was comparable across the 23 donors (Figure S14). The heat map in Figure 6A illustrates that the personalized coronas formed from 23 donors exhibited distinct proteomic profiles with different protein composition and abundance. Specifically, the proteins that were predominant in the personalized coronas differed from the proteins that were the most abundant in neat plasma (Figure 6B). The most abundant corona proteins histidine-rich glycoprotein (HRG) and apolipoprotein B-100 (APOB) (identified in the personalized coronas) exhibited an average of 43- and 4-fold enrichment relative to their abundance in the corresponding neat plasma. In contrast, the LFQ intensity of albumin (ALB) identified on particles in the personalized coronas was 46-fold less than that found in plasma.

Abundance of Specific Proteins Correlates to Particle Association with Monocytes and B Cells. Although the total number of corona proteins varied significantly across 23 donors, it did not correlate with monocyte or B cell association (Figure S15). To identify the key corona proteins that regulate the donor-dependent particle–immune cell association, we further examined the influence of the abundance of each protein identified in the coronas. Using a spearman correlation analysis, we determined the correlation between particle association and each corona protein abundance across the 23 donors (Figure 7A,B). Of the hundreds of proteins identified from the personalized coronas on PEG-MS-100 nanoparticles, only 11 and 8 proteins significantly correlated with monocyte and B cell association, respectively (Table 1), with immunoglobulins (IGKV2-29, IGHV4-34, IGHG1) and complement proteins (C4B, C3) as the top positively

correlating proteins. In contrast, the abundance of apolipoproteins APOA4 and APOE negatively correlated with particle association with either monocytes or B cells (Figure 7A,B). This finding is consistent with current literature on key proteins identified for immune recognition. Immunoglobulins (antibodies) working with the complement system promote phagocytic uptake of opsonized foreign materials,[40,41] whereas apolipoproteins as dysopsonins have been suggested to limit phagocytosis possibly through competitive surface binding with opsonins.[42,43] The protein abundance of neat plasma was similarly analyzed (Figure 7C,D). Fewer proteins displayed significant correlation with particle association (Table S6), suggesting that the highly correlated proteins found on the corona were specifically enriched on the nanoparticles.

To further confirm this observation, we compared the abundance of corona proteins on the PEG-MS-100 nanoparticles from the donors that displayed the highest and lowest degree of cell association with monocytes and B cells—these particles with the corresponding coronas are respectively referred to as high or low responders (Figure S16A–D). Consistent with our correlation study discussed earlier, immunoglobulins (IGKV2-29, IGLV2-11) and complement proteins (C4B, C3) were identified as the key proteins that were significantly upregulated in the corona of the high responders compared with the low responders. An enrichment of more than 40-fold of a particular immunoglobulin type *i.e.*, IGKV2-29 was observed from the personalized coronas on the high responders relative to the personalized coronas on the low responders, whereas no significant fold change of plasma protein abundance was observed between the high and low responders (Figure S16E,F). Overall, these findings confirmed that the enrichment of specific proteins (immunoglobulin and complement proteins) in the personalized corona is linked to the donor-dependent particle association with monocytes and B cells.

The interplay of multiple factors likely accounts for the varied immunoglobulin and complement depositions in a person-specific corona. The polyclonal antibody repertoire of each person is unique and shaped by genetic, environmental factors, diet, and immunological history.[44] As antibodies have different properties (including sequences, hydrophobicity, and surface charges), the serum antibody repertoire could have different intrinsic capability to engage with nanoparticles between donors. Furthermore, the differences in complement proteins (*e.g.*, polymorphisms)[45] and distribution of antibody subclass (which differentially engages the complement system)[46] observed between individuals likely explain the differential deposition of complement proteins on particles. Taken together, our study illustrates that individual variance in the blood proteome can influence corona composition and nanoparticle fate.

CONCLUSIONS

We investigated the formation of personalized biomolecular coronas on particles using plasma from a cohort of 23 healthy donors and their impact on particle–immune cell interactions using an *ex vivo* human blood assay. The behavior of PEG-MS-100 and Doxil nanoparticles varied widely in their association with monocytes and B cells across the 23 corona donors examined, whereas PEG particles displayed minimal cell associations, irrespective of the plasma donor. The personalized coronas generated from the plasma of each donor exhibited distinct proteomic fingerprints. The enrichment of specific immunoglobulins (IGKV2-29, IGHV4-34, IGHG1) and complement proteins (C4B, C3) in the personalized coronas was strongly linked to the donor-dependent particle association with monocytes and B cells, as assessed by our correlation studies. Our work suggests that human subjects will vary widely in their response to nanomedicines. Of direct relevance, our work predicts that subjects with serum proteins that bind to Doxil particles, leading to rapid uptake by monocytes and B cells, will experience increased off-target immune

cell toxicity of Doxil. Further mechanistic understanding of the formation and impact of personalized biomolecular coronas will facilitate the rational engineering of nanomaterials to modulate particle–immune cell interactions, driving advances in the delivery and/or active targeting of nanomaterials, while avoiding nonspecific clearance by the immune system.

METHODS

Materials. All chemicals were of analytical grade and used as received without purification. Milli-Q water with a resistivity of greater than 18.2 MΩ cm was obtained from a three-stage Millipore Milli-Q plus 185 purification system (Millipore Corporation, USA). Doxoves®, PEGylated doxorubicin-encapsulated liposomes that contain the same lipid composition and drug/lipid ratio as clinically used liposomal doxorubicin agent (Doxil®) were purchased from FormuMax Scientific Inc. (USA). Cyanine 5 (Cy5)-labeled PS particles with an average size of 100 nm were purchased from Nanocs Inc. (USA). Synthesis of MS particles was performed using tetraethyl orthosilicate (TEOS), poly(acrylic acid) (PAA, M_W ~250 kDa, 35 wt.% solution in water), cetyltrimethylammonium bromide (CTAB), cetyltrimethylammonium tosylate (CTAT), ammonium hydroxide solution (25%), (3-aminopropyl)triethoxysilane (APTES, 99%), ethanol (EtOH), and triethanolamine from Sigma-Aldrich (USA). Synthesis of PEGylated MS (PEG-MS) particles (PEG, poly(ethylene glycol)) was performed using 8-arm-PEG-NH_2 (40 kDa) and 8-arm-PEG-NHS (10 kDa) with a hexaglycerol core structure purchased from JenKem Technology (USA). Silica removal was performed using hydrofluoric acid (HF, 48%) and ammonium fluoride (NH_4F, 98%) from Sigma-Aldrich (USA). Particle labeling was performed using Alexa Fluor 488 succinimidyl ester (AF488-NHS) and Alexa Fluor 647 succinimidyl ester (AF647-NHS) purchased from Life Technologies (USA) and dimethyl sulfoxide (DMSO; anhydrous, >99%) obtained from Sigma-Aldrich (USA). Cell labeling was carried out using Alexa Fluor 594-

conjugated wheat germ agglutinin (WGA-AF594), WGA-AF488, and Hoechst 33342, all purchased from Life Technologies (USA). For purification of PBMCs, Ficoll-Paque PLUS (GE Healthcare, USA) was used. For cell phenotyping, antibodies against CD45 V500 (H130), CD19 BV650 (HIB19), CD14 (MΦP9), CD3 AF700 (SP34-2), and CD56 PE (B159) were used, all purchased from BD Biosciences (USA), except for CD19 BV650 that was obtained from BioLegend (USA). Purification following cell phenotyping was carried out using phosphate-buffered saline (PBS) containing 0.5% w/v BSA, purchased from Sigma-Aldrich (USA), and 2 mM ethylenediaminetetraacetic acid (EDTA) from Life Technology (USA). Cell fixation was carried out using formaldehyde (1% w/v) purchased from Sigma-Aldrich (USA) diluted in PBS.

Synthesis of MS Particles. MS-800 particles were synthesized using polyelectrolyte–surfactant complexes as templates.[31] Briefly, after dissolving CTAB (2.2 g) in Milli-Q water (50 mL), PAA solution (8.5 g) and ammonium hydroxide solution (8.1 mL) were added under vigorous stirring. After incubation for 20 min, TEOS (8.92 mL) was added to the reaction solution, followed by further stirring for 15 min. The mixture was transferred to a Teflon-sealed autoclave, which was heated at 100 °C for 48 h. The synthesized particles were purified by washing with water and EtOH three times, followed by calcination at 550 °C in air for 24 h. MS-450 particles was synthesized following the same protocol except that the PAA amount was reduced to 6 g. MS-100 particles were synthesized following a published method.[32] After dissolving CTAT (960 mg) and triethanolamine (174 mg) in Milli-Q water (50 mL) at 80 °C, TEOS (7.8 mL) was added to the solution, followed by 2 h incubation under vigorous stirring. The resulting particles were washed with water and EtOH three times, followed by calcination at 550 °C in air for 24 h. To fluorescently label the particles, MS particles were functionalized with amine groups, followed by conjugation of AF647/AF488-NHS to the amine groups and capping with TEOS. The particles (18 mg) were

dispersed in EtOH (1 mL), followed by addition of ammonium hydroxide solution (3 µL) and APTES (3 µL, 10× diluted in EtOH). After incubation for 18 h at 22 °C under stirring and washing in EtOH and DMSO (anhydrous) three times, the particles were dispersed in DMSO (300 µL) and AF647/AF488-NHS (10 µL, 1 mg mL^{-1} in DMSO) was added. After incubation for 10 h at 22 °C under stirring, excess dye was removed by washing with DMSO and EtOH three times. The particles were dispersed in EtOH (300 µL) and ammonium hydroxide solution (4 µL) and TEOS (4 µL) were added. After incubation for 18 h at 22 °C under stirring, the particles were washed with EtOH and Milli-Q water three times. The particles were stored in Milli-Q water at 4 °C prior to use.

Synthesis of PEG-MS and PEG Particles. PEG-MS particles were synthesized using a published method.[27] Briefly, 8-arm PEG NH_2 (2.4 mg) was infiltrated into MS particles (6 mg) in 480 µL phosphate buffer (100 mM, pH 8) under mild stirring for 18 h, followed by washing three times with the phosphate buffer. The particles were subsequently dispersed in 8-arm PEG NHS solution (400 µL, 2 mg mL^{-1} in phosphate buffer) to cross-link the PEG networks. To label the PEG-MS particles, AF647/AF488-NHS (10 µL, 1 mg mL^{-1} in DMSO) was added during the cross-linking step. After incubation for 3 h under mild stirring, the PEG-MS particles were washed with Milli-Q water and stored in Milli-Q water at 4 °C prior to use. To obtain PEG particles, the MS templates were dissolved with a HF (2 M)/NH_4F (8 M) solution (pH 5), followed by washing three times with Milli-Q water. *Caution! HF is highly toxic. Extreme care should be taken when handling HF solution and only small quantities should be prepared*. The PEG particles were stored in Milli-Q water at 4 °C prior to use.

Particle Characterization. TEM images were acquired using an FEI Tecnai TF20 instrument at an operation voltage of 120 kV under liquid nitrogen cooling. Particle suspensions were dropped

and air-dried on formvar carbon-coated copper grids (plasma-treated). PEG-100 nanoparticles were negatively stained with 1% uranyl acetate in Milli-Q water before TEM measurement. Fluorescence microscopy images of AF647-labeled MS-800, MS-450, PEG-MS-800, PEG-MS-450, PEG-800, and PEG-450 particles were acquired with a Nikon A1R confocal microscope with a standard FITC/TRITC/CY5 filter set. Super-resolution fluorescence microscopy images of AF488-labeled MS-100, PEG-MS-100, and PEG-100 particles were taken with a DeltaVision OMX super-resolution structured illumination microscope (Applied Precision, USA). DLS analysis of the particles was performed on a Zetasizer Nano-ZS (Malvern Instruments, UK) instrument. Particles without or with a biomolecular corona were formed by incubating with PBS or human plasma for 1 h at 37 °C, followed by washing three times with PBS before measurement. As the PEG particles minimally scattered light, the size of these particles was determined by fluorescence microscopy (Figure S1). Zeta potential measurements of the particles were performed at pH 7.3 in phosphate buffer (2 mM) using a Zetasizer Nano-ZS (Malvern Instruments, UK) instrument. Particle counting for MS-800, MS-450, PEG-MS-800, PEG-MS-450, PEG-800, and PEG-450 particles was performed using an Apogee A50-Micro flow cytometer (Apogee Flow Systems, UK). Particle counting for MS-100, PEG-MS-100, and PEG-100 nanoparticles could not be accurately performed by flow cytometry owing to their small size. Instead, the mass of these particles was determined by weighting the freeze-dried particles. The concentration of MS-100 particles was estimated *via* nanoparticle tracking analysis performed on a Malvern NanoSight NS400 instrument fitted with a 405 nm laser (65 mW output).

Assays Using Human Plasma and PBMCs. Fresh blood was collected from 23 healthy human volunteers into sodium heparin vacuettes (Greiner Bio-One) after obtaining informed consent in accordance with The University of Melbourne Human Ethics Approval #1443420 and the

Australian National Health and Medical Research Council Statement on Ethical Conduct in Human Research. Plasma was prepared by centrifuging blood (900 *g*, 15 min, without brake) and collecting the top layer. The centrifugation step was repeated to remove any remaining cells in the plasma. Plasma from the 23 healthy donors were aliquoted and stored at −80 °C before use. Heat-inactivation of plasma was performed by heating plasma at 56 °C for 30 min. PBMCs were collected from fresh human blood using density gradient centrifugation with Ficoll-Paque PLUS (GE Healthcare, USA). The obtained PBMCs were subsequently washed four times with RPMI 1640 (serum-free) medium to remove any residual plasma proteins. The absence of plasma proteins was confirmed by the lack of absorbance of the supernatant at 280 nm (Nanodrop 2000, Thermo Fisher Scientific, USA). Cell counts were conducted with a CELL-DYN Emerald analyzer (Table S7). Fresh PBMCs were used in each experiment.

Blood Assay to Determine Particle Association with Human Immune Cells. The purified PBMCs from fresh human blood were suspended in RPMI 1640 (serum-free) medium on ice. Particles (5×10^8 or 2 μg) were pre-incubated in PBS or plasma (100 μL) at 37 °C for 1 h. Individual plasma from 23 healthy donors were used to form personalized coronas. The particles (2.5×10^7 or 0.1 μg) with either no corona or a personalized corona were added to PBMCs (5×10^5) in RPMI 1640 medium (serum-free, 100 μL) at a cell-to-particle ratio of 1:50 or particle dosage of 1 μg mL^{-1}. For MS-100 particles, the particle dosage of 1 μg mL^{-1} corresponds to a cell-to-particle ratio of ~1:300 (estimated by nanoparticle tracking analysis). Particle dosage was varied by pre-diluting concentrated particle suspensions with PBS. After incubation for 1 h at 37 °C, PBMCs were washed with PBS (4 mL, 500 *g*, 7 min) and phenotyped in PBS at 4 °C for 1 h using titrated concentration of antibodies against CD45 V500 (H130, BD), CD19 BV650 (HIB19, BioLegend), CD14 (MΦP9, BD), CD3 AF700 (SP34-2, BD), and CD56 PE (B159, BD). Unbound

antibodies were removed by washing twice with cold (4 °C) PBS containing 0.5% w/v BSA and 2 mM EDTA (4 mL, 500 *g*, 7 min). Cells were fixed with 1% w/v formaldehyde in PBS and directly analyzed by flow cytometry (LSRFortessa, BD Biosciences) and data was processed using FlowJo V10.

Cell Sorting and Imaging. After particle incubation with PBMCs for 1 h at 37 °C as described in *Blood Assay to Determine Particle Association with Human Immune Cells*, untouched B cells and monocytes were isolated from PBMCs by immunomagnetic negative selection using the EasySep™ Human B Cell Isolation Kit (STEMCELL Technology, Canada) and Pan Human Monocyte Isolation Kit (Miltenyi Biotec, Germany), respectively. Following manufacturer's protocol, the proportion of B cells and monocytes from the isolated fractions was about 95% and 74%, respectively (Figure S17).

Each slide of a 8-well Lab-Tek chambered coverglass slide (Thermo Fisher Scientific, USA) was treated with poly-L-lysine (200 µL, 0.01% w/v, M_w 70–150 kDa) solution for 2 h at 22 °C, followed by washing with PBS and air-drying. The sorted monocytes and B cells (1×10^5) were added to each well, allowed to set in the dark for 1 h at 22 °C, and fixed with 4% paraformaldehyde in PBS (200 µL) for 20 min. Cell membranes were subsequently stained with WGA-AF488 or WGA-AF594 (5 µg mL^{-1} in PBS) at 4 °C for 5 min, followed by washing twice with PBS (400 µL). Cell nuclei were stained with Hoechst 33342 (5 µg mL^{-1} in PBS) for 20 min at 22 °C, followed by washing twice with PBS (400 µL). The stained cells were covered with VECTASHIELD antifade mounting medium (Vector Laboratories, USA) and stored at 4 °C before imaging. Fluorescence microscopy images of cells were obtained on a Nikon A1R confocal microscope equipped with a 60× oil immersion objective and a standard DAPI/FITC/TRITC/CY5 filter set. Super-resolution images were acquired on a DeltaVision OMX structured illumination microscope

(Applied Precision) operating in SIM mode to obtain approximate resolution of 110 nm in *X*/*Y* and 250 nm in *Z*.

Incubation of Particles in Human Plasma for Proteomics Analysis. PEG-MS-100 nanoparticles (200 μg) were incubated in plasma (500 μL) from 23 healthy donors for 1 h at 37 °C. After incubation, the nanoparticles were washed four times with PBS (10000 *g*, 10 min) at 4 °C. The obtained biomolecular corona-coated particles were stored at −80 °C before proteomics analysis.

Mass Spectrometry Analysis. Neat plasma samples and corona-coated particles were prepared for mass spectrometry analysis using the USP[3] method as previously described,[47] with some modifications. Briefly, the corona-coated particles were transferred to a 0.5 mL LoBind deep well plate (Eppendorf) and subjected to reduction/alkylation in preheated (95 °C) sodium dodecyl sulfate (SDS) lysis buffer (5% SDS/10 mM tris/10 mM tris(2-carboxyethyl)phosphine/5.5 mM 2-chloroacetamide) for 3 min. The corona-coated particles were incubated in acetonitrile (ACN; 100 μL, final concentration, 70% v/v) at room temperature for 20 min. Samples were then centrifuged at 13,000 *g* (Hitachi CR21G) for 5 min at room temperature. The supernatants were discarded, and the particles were washed twice with 70% EtOH (150 μL) and once with neat ACN (150 μL). ACN was completely evaporated from the tubes using a CentriVap (Labconco) before addition of the digestion buffer (40 μL, 10% trifluoroethanol/100 mM NH_4HCO_3) containing Lys-C (Wako, 129-02541) and Trypsin Gold (Promega, V5280) (1 μg total enzyme). Enzymatic digestion proceeded for 1.5 h at 37 °C using the ThermoMixer C (Eppendorf) shaking at 400 rpm. After digestion, the supernatants containing peptides were collected, and an additional elution (50 μL) was performed with 2% DMSO before sonication in a water bath for 1 min. The eluates were combined and transferred to the top of pre-equilibrated C18 StageTips (2× plugs of 3 M Empore resin, #2215)

for sample cleanup as previously described.[48] The eluates were lyophilized to dryness using a CentriVap (Labconco) prior to reconstituting in 0.1% formic acid (FA)/2% ACN (40 µL) for mass spectrometry analysis. For the neat plasma samples, 5% SDS lysis buffer (37.5 µL) was added to neat plasma (2.5 µL) and subjected to reduction/alkylation at 95 °C for 10 min. An aliquot (5 µL) of diluted plasma was combined with pre-washed PureCube Carboxy Agarose Magbeads (20 µL) (Cube Biotech, Germany, Cat #50225), followed by the addition of ACN, resulting in a final concentration of 70% v/v. The samples were subjected to the USP[3] protocol as described above, with the following exceptions: the beads were placed on a magnetic rack to wash the beads and remove the peptide supernatant, total enzyme (2 µg) was used for the digestion of neat plasma, and C18 StageTips (3× plugs of 3 M Empore resin, #2215) were prepared for sample cleanup. The eluates were lyophilized to dryness using a CentriVap (Labconco) prior to reconstituting in 0.1% FA/2% ACN (35 µL) for mass spectrometry analysis. Peptides were analyzed using a nanoElute (Bruker, Germany) coupled to a timsTOF Pro (Bruker) equipped with a CaptiveSpray source. Peptides (1 µL) derived from the corona-coated particles or neat plasma were separated on a 15 cm × 75 µm analytical column, 1.6 µm C18 beads with a packed emitter tip (IonOpticks, Australia). The column temperature was maintained at 50 °C using an integrated column oven (Sonation GmbH, Germany). For analysis of the corona-coated particles, the column was equilibrated using 4 column volumes before sample loading in 100% buffer A (99.9% Milli-Q water, 0.1% FA) (both steps performed at 980 bar). Samples were separated at 400 nL min^{-1} using a linear gradient from 2 to 24% buffer B (99.9% ACN, 0.1% FA) over 47 min before ramping to 34% buffer B (6 min) and to 80% buffer B (6 min), and maintaining for 6 min (total separation method time was 65 min). Peptides derived from neat plasma samples were separated at 400 nL min^{-1} using a linear gradient

from 5 to 30% buffer B (99.9% ACN, 0.1% FA) over 16.8 min before ramping to 95% buffer B (0.5 min) and maintaining for 2.4 min (total separation method time was 19.7 min).

Mass Spectrometry Data Analysis. Raw files consisting of high-resolution mass spectra were processed with MaxQuant (version 1.6.6.0) for feature detection and protein identification using the Andromeda search engine[49] as previously described.[50] Extracted peak lists were searched against the reviewed *Homo sapiens* (UniProt, March 2019) database as well as a separate reverse decoy database to empirically assess the false discovery rate (FDR) using strict trypsin specificity, allowing up to 2 missed cleavages. LFQ was selected, with a minimum ratio count of 2. Peptide-spectrum match and protein identifications were filtered using a target–decoy approach at an FDR of 1%. Only unique and razor peptides were considered for quantification with intensity values present in at least half of the replicates per group. Statistical analyses were performed using LFQAnalyst[51] (https://bioinformatics.erc.monash.edu/apps/LFQ-Analyst/) whereby the LFQ intensity values were used for protein quantification. Missing values were replaced by values drawn from a normal distribution of 1.8 standard deviation and a width of 0.3 for each sample (Perseus-type). Protein-wise linear models combined with empirical Bayes statistics were used for differential expression analysis using Bioconductor package Limma whereby the adjusted *p*-value cutoff was set at 0.05 and the $\log_2$ fold change cutoff was set at 1. The Benjamini–Hochberg (BH) method of FDR correction was used. Heat maps were generated with heatmapper (http://www.heatmapper.ca/)[52] using the arithmetic mean of the LFQ intensity in the replicates of each sample.

Spearman Correlation Analysis. Spearman correlation coefficients were calculated across triplicate values from 23 donors using *cor.test* function from *R* (v3.6.3) by specifying *spearman* in the argument. The FDR was controlled by adjusting the *p*-values using the BH adjustment. This

was done by calling the *p.adjust* function (using *method=BH*) from *R* (v3.6.3). *p*-Values of less than 0.05 were considered significant.

Minimum Information Reporting in Bio–Nano Experimental Literature (MIRIBEL). The studies conducted herein, including material characterization, biological characterization, and experimental details, conform to the MIRIBEL reporting standard for bio–nano research,[53] and we include a companion checklist of these components in the Supporting Information.

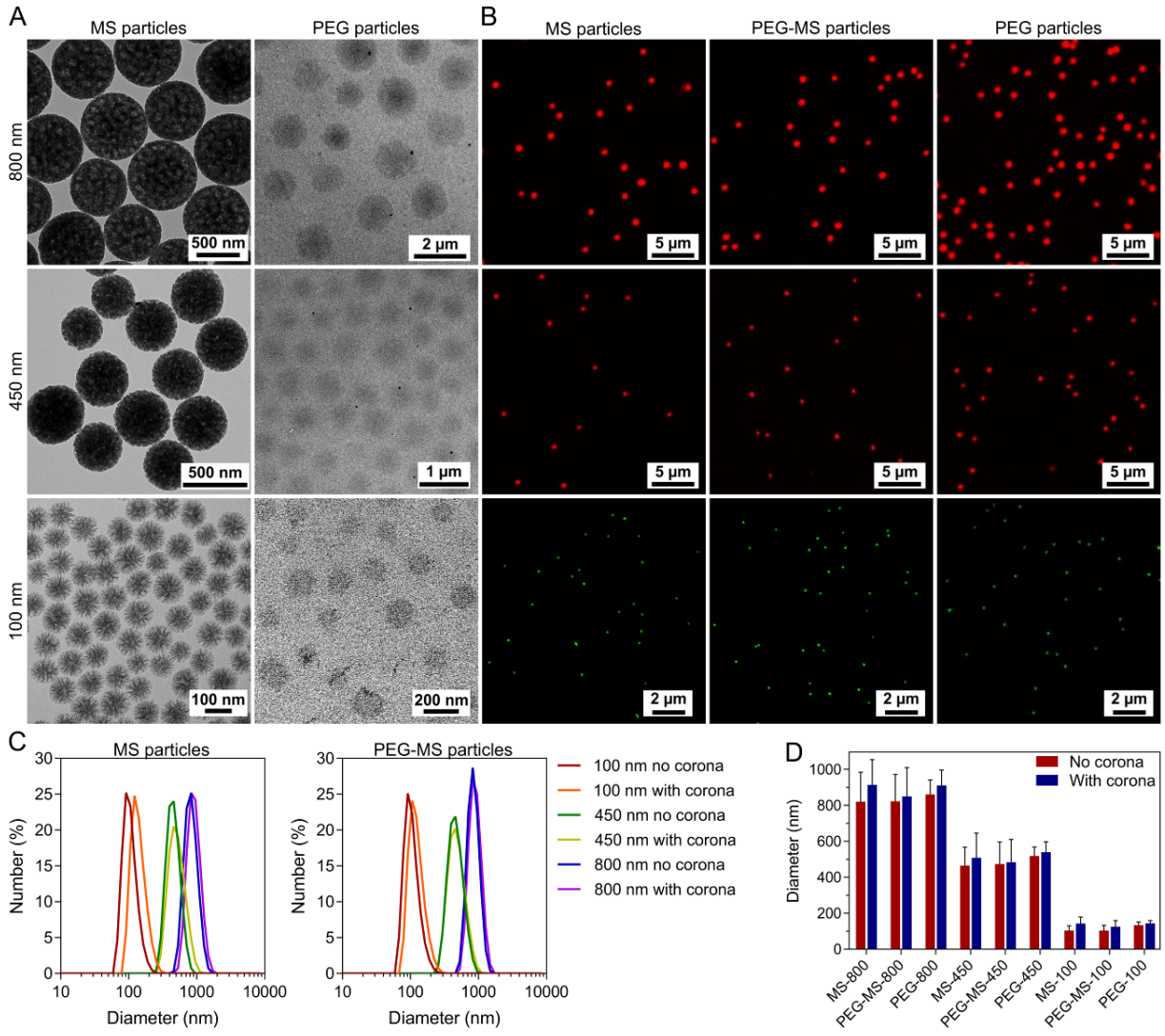

Figure 1. Characterization of MS, PEG-MS, and PEG particles of three different sizes (800, 450, and 100 nm). (A) Transmission electron microscopy (TEM) images of MS and PEG particles. (B) Fluorescence microscopy images of fluorescently labeled MS, PEG-MS, and PEG particles suspended in human plasma. (C) Dynamic light scattering (DLS) of MS and PEG-MS particles without and with biomolecular coronas. (D) Diameter of MS, PEG-MS, and PEG particles without and with biomolecular coronas. The sizes of the MS and PEG-MS particles were determined by DLS, presented as the mean ± standard deviation (SD) of three independent measurements. As PEG particles have minimal light scattering, the size of the particles was determined by

fluorescence microscopy (Figure S1), shown as the mean ± SD (n = 20). No significant difference in size of each particle with “no corona” and “with corona” (two-way ANOVA with Tukey’s multiple comparisons test) was observed.

Scheme 1. Schematic Illustration of the *Ex Vivo* Human Blood Assay.[a]

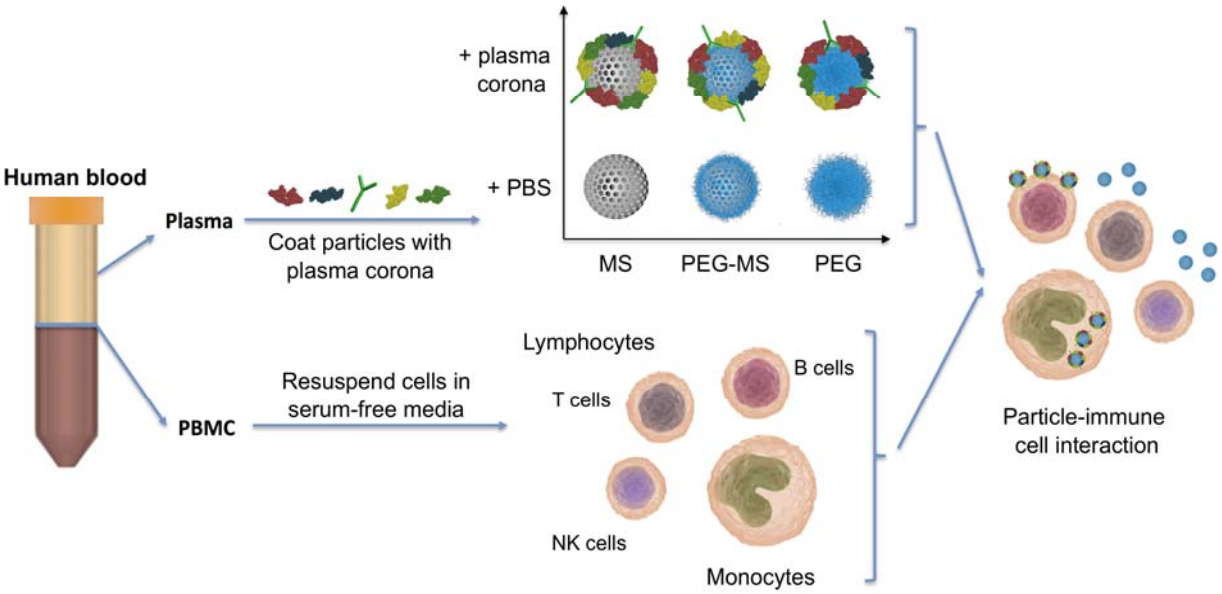

[a]Plasma and peripheral blood mononuclear cells (PBMCs, including lymphocytes and monocytes) are separated from fresh human blood. PBMCs are washed and suspended in serum-free media. Particles are pre-incubated with either plasma or phosphate-buffered saline (PBS) and then incubated with PBMCs in serum-free media for 1 h at 37 °C, followed by phenotyping cells with antibody cocktails and analysis by flow cytometry. The schematic representation of PBMCs was adapted with permission from ref 35. Copyright 2017 American Chemical Society.

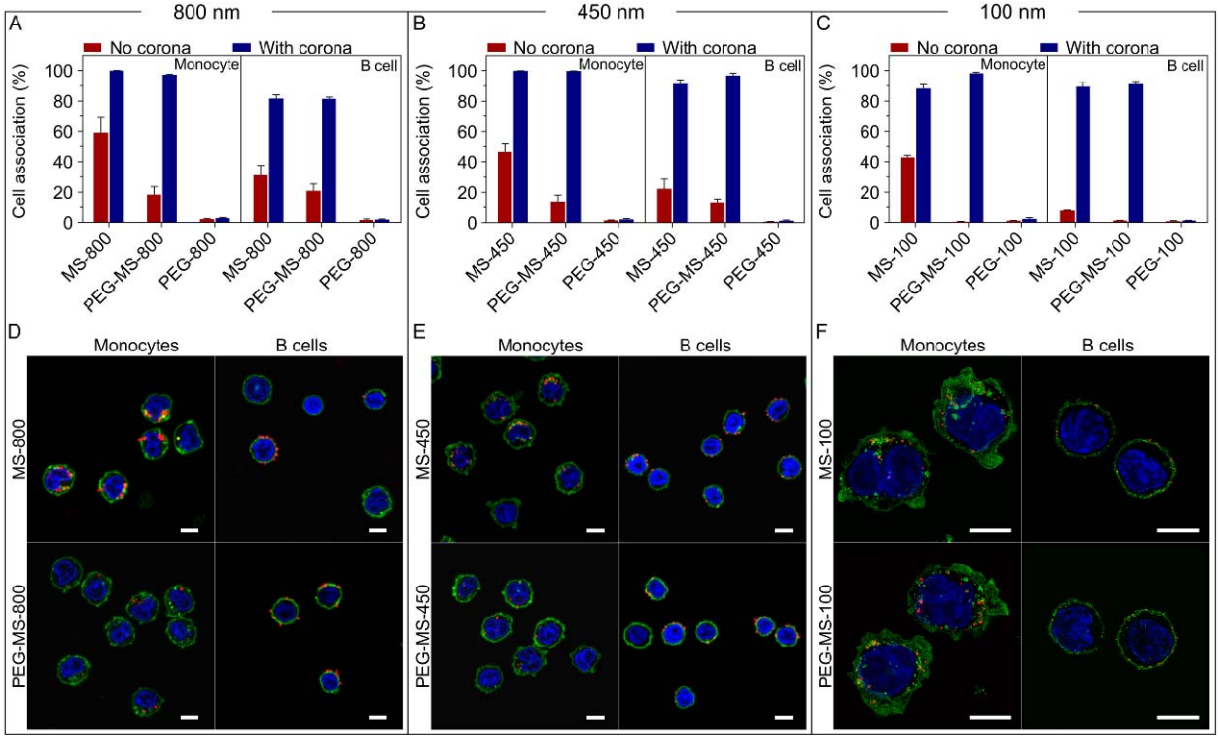

Figure 2. Corona effect on particle–immune cell interaction study using plasma and PBMCs from one donor. (A–C) Association of MS-800, PEG-MS-800, and PEG-800 (A), MS-450, PEG-MS-450, and PEG-450 (B), and MS-100, PEG-MS-100, and PEG-100 (C) particles with monocytes and B cells. Particles without or with corona were formed by pre-incubating with PBS or human plasma from a healthy donor before incubating with autologous PBMCs in serum-free media. Cell association (%) refers to the proportion of each cell type with positive fluorescence, above background, stemming from AF647-labeled particles (see gating strategy in Figure S2). Data are shown as the mean ± SD of three independent experiments (using the same batch of plasma from a single donor), with at least 100,000 leukocytes analyzed for each experimental condition. The results from statistical analysis are presented in Figure S3. (D–F) Cross-sectional fluorescence microscopy images to assess particle internalization by monocytes and B cells. (D) MS-800 or PEG-MS-800, (E) MS-450 or PEG-MS-450, and (F) MS-100 or PEG-MS-100 particles were pre-incubated with human plasma from a healthy donor before incubating with autologous PBMCs in

serum-free media. After incubation, monocytes and B cells were sorted from PBMCs and imaged by (D,E) confocal microscopy and (F) super-resolution fluorescence microscopy. In (D,E), particles were labeled with AF647 (red) and cell membranes were stained with Alexa Fluor 488-conjugated wheat germ agglutinin (WGA-AF488) (green). In (F) particles were labeled AF488 (red) and cell membranes were stained with WGA-AF594 (green). In (D–F), cell nuclei were stained with Hoechst 33342 (blue). Scale bars are 5 μm.

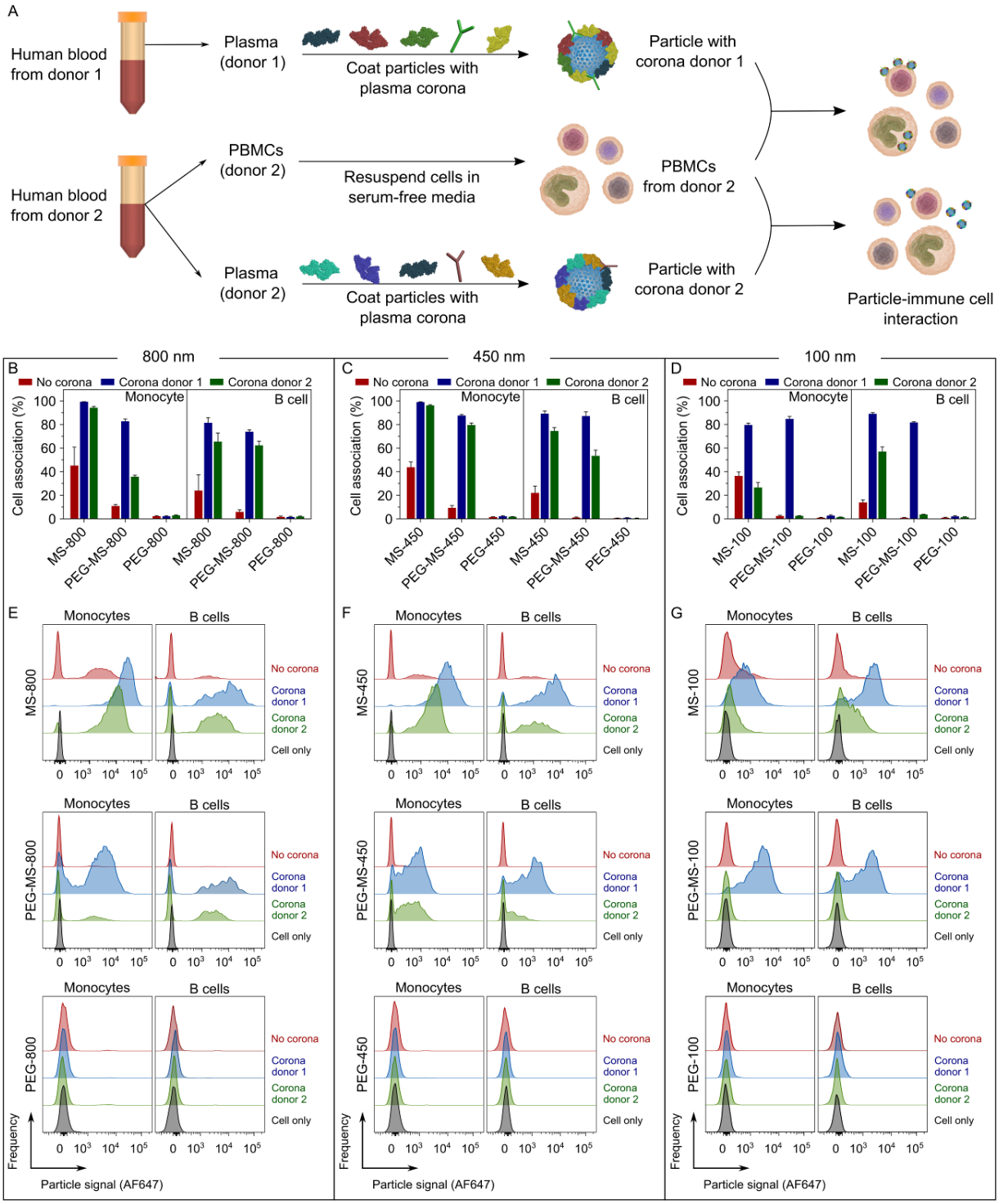

Figure 3. Effect of corona donor on particle–immune cell interaction. (A) Schematic illustration of the blood assay performed using two sets of plasma from healthy donor 1 and donor 2 and PBMCs from donor 2. Particles were pre-incubated with plasma from donor 1 or donor 2 to form

personalized coronas before adding them to washed PBMCs from donor 2 in serum-free media. The schematic representation of the PBMCs was adapted with permission from ref 35. Copyright 2017 American Chemical Society. (B–D) Association of MS-800, PEG-MS-800, and PEG-800 (B), MS-450, PEG-MS-450, and PEG-450 (C), and MS-100, PEG-MS-100, and PEG-100 (D) particles with monocytes and B cells. Cell association (%) refers to the proportion of each cell type with positive fluorescence, above background, stemming from AF647-labeled particles. Data are shown as the mean ± SD of three independent experiments (using the same batch of plasma from each donor), with at least 100,000 leukocytes analyzed for each experimental condition studied. The statistical analysis data are presented in Figure S5. (E–G) Flow cytometry histograms represent association of MS-800, PEG-MS-800, and PEG-800 (E), MS-450, PEG-MS-450, and PEG-450 (F), and MS-100, PEG-MS-100, and PEG-100 (G) particles with monocytes and B cells. Particles were pre-incubated with either PBS or plasma from donor 1 or donor 2 before incubating with washed PBMCs from donor 2 in serum-free media. Cell only control groups show the respective cell populations without particles in the incubation media.

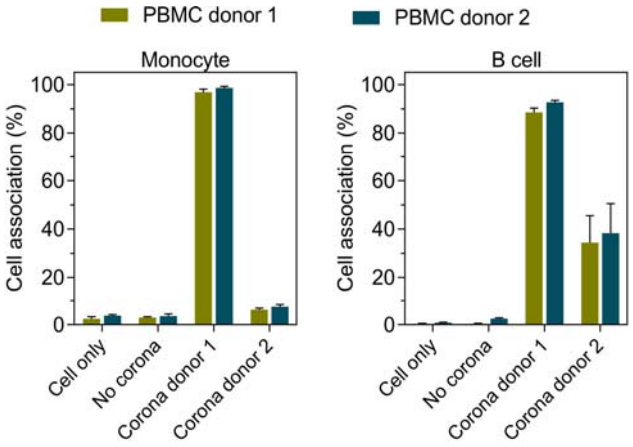

Figure 4. Comparison of the impact of corona donor variance with PBMC donor variance on particle–immune cell association. PEG-MS-100 nanoparticles were pre-incubated with either PBS or plasma from donor 1 or donor 2 before incubating with washed PBMCs from donor 1 or donor 2 (see Figure S8 for experiment setup). Cell association (%) refers to the proportion of each cell type with positive fluorescence, above background, stemming from AF647-labeled particles. Data are shown as the mean ± SD of three independent experiments (using the same batch of plasma from each donor), with at least 100,000 leukocytes analyzed for each experimental condition studied. Cell only control groups represent the respective cell populations without particles in the incubation media. Full statistical data are presented in Figure S9.

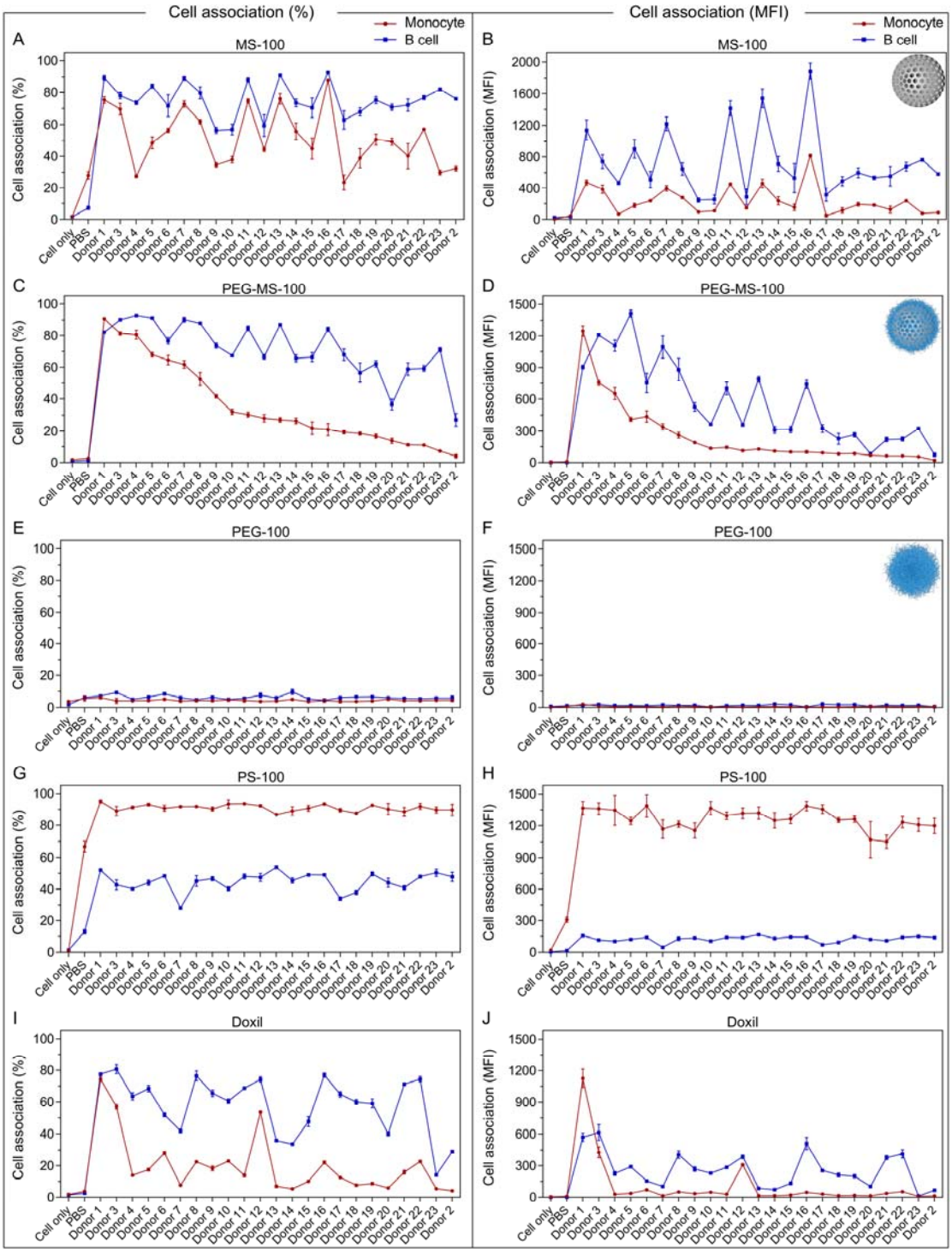

Figure 5. Impact of the personalized corona on particle–immune cell interactions. (A,B) MS-100, (C,D) PEG-MS-100, (E,F) PEG-100, (G,H) PS-100, or (I,J) Doxil nanoparticles were pre-incubated in either PBS or plasma from 23 healthy donors before incubating with washed PBMCs

from donor 2 in serum-free media. Cell association (%) refers to the proportion of each cell type with positive fluorescence, above background, stemming from AF647-labeled particles. Cell association (MFI) refers to the median AF647 fluorescence index of each cell type. Data are shown as the mean ± SD of three independent experiments (using the same batch of plasma from each donor), with at least 100,000 leukocytes analyzed for each experimental condition studied. Cell only control groups represent the respective cell populations without particles in the incubation media. Donor numbers 3–23 are arranged based on PEG-MS-100 nanoparticle association with monocytes (from high to low) for easy comparison across different particles.

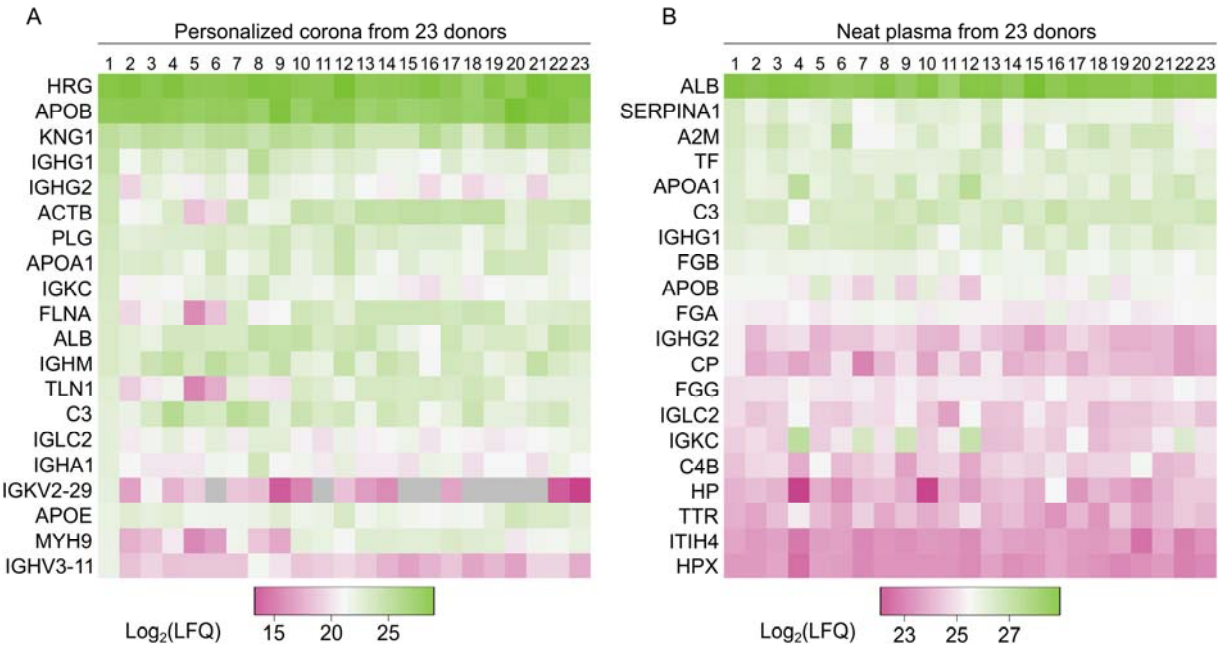

Figure 6. Heat map of the top 20 proteins identified in (A) the personalized coronas of PEG-MS-100 nanoparticles treated with plasma from 23 healthy human donors and (B) the neat plasma from 23 healthy human donors. In the heat map, purple and green indicate low and high label-free quantification (LFQ) intensities (log_2(LFQ)), respectively, as shown by the color scale bar. Gray regions indicate that a given protein was not identified in the sample. The LFQ intensity values of the top 20 proteins are provided in Tables S2 and S3.

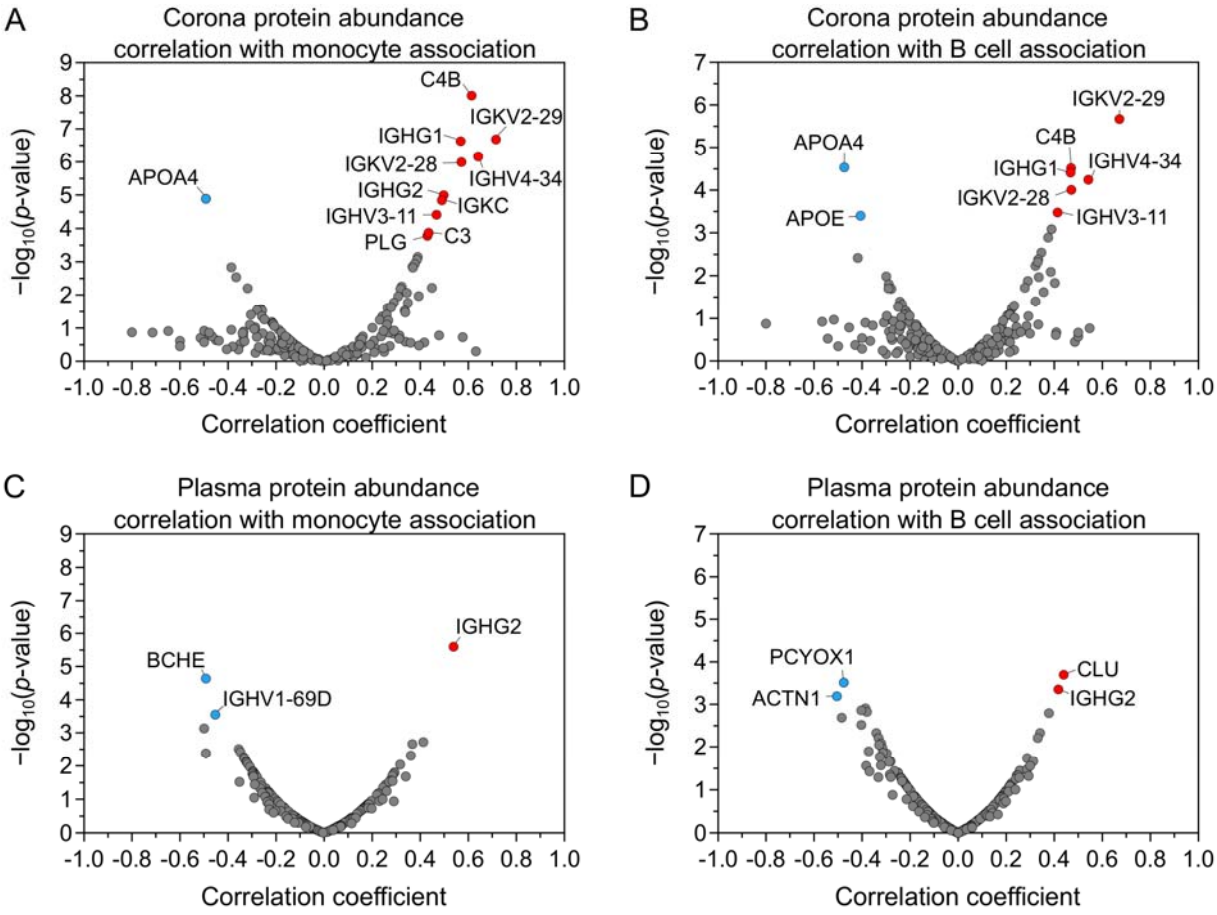

Figure 7. Spearman correlation analysis of protein abundance on personalized biomolecular coronas and neat plasma from 23 healthy donors with cell association. (A,B) Volcano plots of significance ($-\log_{10}(p\text{-value})$) *versus* correlation coefficient identifying the key proteins within the biomolecular coronas that are highly correlated with PEG-MS-100 nanoparticle association with monocytes (A) and B cells (B). (C,D) Changes in protein abundance in the plasma from 23 donors were used as control to compare against the corona-specific proteins. The top proteins that have a significant correlation (correlation coefficient of ≥0.4 and Benjamini–Hochberg-adjusted *p*-value of ≤0.05) are presented as red or blue dots (positive or negative correlation, respectively). The key identified proteins are listed in Table 1.

Table 1. Key proteins identified from the 23 personalized biomolecular coronas of PEG-MS-100 nanoparticles showing significant correlation (correlation coefficient of ≥0.4 and Benjamini–Hochberg-adjusted *p*-value of ≤0.05) with cell association (MFI) with monocytes and B cells[a]

	Uniprot ID	Gene Name	Protein Name	Correlation Coefficient	$-\text{Log}_{10}$(*p*-value)
Correlation with monocyte association (MFI)	A2NJV5	IGKV2-29	Immunoglobulin kappa variable 2-29	0.72	6.68
	P06331	IGHV4-34	Immunoglobulin heavy variable 4-34	0.64	6.16
	A0A140TA29	C4B	Complement C4-B	0.61	8.00
	P01857	IGHG1	Immunoglobulin heavy constant gamma 1	0.57	6.63
	A0A075B6P5	IGKV2-28	Immunoglobulin kappa variable 2-28	0.57	6.00
	P01859	IGHG2	Immunoglobulin heavy constant gamma 2	0.50	5.00
	P01834	IGKC	Immunoglobulin kappa constant	0.49	4.85
	P01762	IGHV3-11	Immunoglobulin heavy variable 3-11	0.47	4.41
	P01024	C3	Complement C3	0.43	3.87
	P00747	PLG	Plasminogen	0.43	3.78
	P06727	APOA4	Apolipoprotein A-IV	−0.49	4.89
Correlation with B cell association (MFI)	A2NJV5	IGKV2-29	Immunoglobulin kappa variable 2-29	0.67	5.67
	P06331	IGHV4-34	Immunoglobulin heavy variable 4-34	0.54	4.24
	A0A140TA29	C4B	Complement C4-B	0.47	4.51
	P01857	IGHG1	Immunoglobulin heavy constant gamma 1	0.47	4.41
	A0A075B6P5	IGKV2-28	Immunoglobulin kappa variable 2-28	0.47	4.01
	P01762	IGHV3-11	Immunoglobulin heavy variable 3-11	0.41	3.48
	P06727	APOA4	Apolipoprotein A-IV	−0.47	4.53
	P02649	APOE	Apolipoprotein E	−0.41	3.40

[a]Proteins highlighted in blue indicate negative correlation and proteins highlighted in orange indicate positive correlation. MFI, median fluorescence intensity.

ASSOCIATED CONTENT

Supporting Information. Experimental details, particle characterization, statistical analysis of flow cytometry data, mass spectrometry data, and MIRIBEL checklist for reporting research in bio−nano science. This material is available free of charge *via* the Internet at http://pubs.acs.org.

The authors declare no competing financial interest.

AUTHOR INFORMATION

Corresponding Authors

*Email: fcaruso@unimelb.edu.au.

*Email: skent@unimelb.edu.au.

ORCID

Yi Ju: 0000-0003-0103-1207

Hannah G. Kelly: 0000-0002-4652-5609

Laura F. Dagley: 0000-0003-4171-3712

Arnold Reynaldi: 0000-0002-5529-5542

Craig A. Bell: 0000-0002-8986-2795

Jiwei Cui: 0000-0003-1018-4336

Andrew J. Mitchell 0000-0003-4454-853X

Zhixing Lin: 0000-0001-9372-3424

Adam K. Wheatley 0000-0002-5593-9387

Kristofer J. Thurecht: 0000-0002-4100-3131

Miles P Davenport: 0000-0002-4751-1831

Andrew Webb: 0000-0001-5061-6995

Frank Caruso: 0000-0002-0197-497X

Stephen J. Kent: 000-0002-8539-4891

ACKNOWLEDGMENT

This work was conducted and funded by the Australian Research Council Centre of Excellence in Convergent Bio-Nano Science and Technology (project number CE140100036). F.C. acknowledges the award of an NHMRC Senior Principal Research Fellowship (GNT1135806), Y.J. acknowledges the award of an Early Career Researcher Grant from The University of Melbourne (ECR1032020), and J.C. acknowledges the National Natural Science Foundation of China (Nos. 21603120 and 21872085). This work was performed in part at the Materials Characterisation and Fabrication Platform (MCFP) at The University of Melbourne and the Victorian Node of the Australian National Fabrication Facility (ANFF). Transmission electron microscopy analyses were conducted using the facilities at the Biosciences Microscopy Unit, School of Bioscience, The University of Melbourne. The authors acknowledge M. McLean, S. Alcantara, T. Amarasena, P. Brannon, J. Glass, and M. Faria for helpful discussions. All experiments were performed in accordance with the guidelines of the Australian National Health and Medical Research Council Statement on Ethical Conduct in Human Research and the experiments were approved by the Human Ethics Committee at The University of Melbourne (#1443420). Informed consents were obtained from human participants of this study.

REFERENCES

(1) Lim, E.-K.; Kim, T.; Paik, S.; Haam, S.; Huh, Y.-M.; Lee, K. Nanomaterials for Theranostics: Recent Advances and Future Challenges. *Chem. Rev.* **2015**, *115*, 327–394.

(2) Wilhelm, S.; Tavares, A. J.; Dai, Q.; Ohta, S.; Audet, J.; Dvorak, H. F.; Chan, W. C. W. Analysis of Nanoparticle Delivery to Tumours. *Nat. Rev. Mater.* **2016**, *1*, 16014.

(3) Lundqvist, M.; Stigler, J.; Elia, G.; Lynch, I.; Cedervall, T.; Dawson, K. A. Nanoparticle Size and Surface Properties Determine the Protein Corona with Possible Implications for Biological Impacts. *Proc. Natl. Aca. Sci. U. S. A.* **2008**, *105*, 14265–14270.

(4) Docter, D.; Westmeier, D.; Markiewicz, M.; Stolte, S.; Knauer, S. K.; Stauber, R. H. The Nanoparticle Biomolecule Corona: Lessons Learned – Challenge Accepted? *Chem. Soc. Rev.* **2015**, *44*, 6094–6121.

(5) Mahmoudi, M.; Bertrand, N.; Zope, H.; Farokhzad, O. C. Emerging Understanding of the Protein Corona at the Nano-Bio Interfaces. *Nano Today* **2016**, *11*, 817–832.

(6) Caracciolo, G.; Farokhzad, O. C.; Mahmoudi, M. Biological Identity of Nanoparticles *in Vivo*: Clinical Implications of the Protein Corona. *Trends Biotechnol.* **2017**, *35*, 257–264.

(7) Walkey, C. D.; Chan, W. C. Understanding and Controlling the Interaction of Nanomaterials with Proteins in a Physiological Environment. *Chem. Soc. Rev.* **2012**, *41*, 2780–2799.

(8) Monopoli, M. P.; Aberg, C.; Salvati, A.; Dawson, K. A. Biomolecular Coronas Provide the Biological Identity of Nanosized Materials. *Nat. Nanotecnol.* **2012**, *7*, 779–786.

(9) García-Álvarez, R.; Hadjidemetriou, M.; Sánchez-Iglesias, A.; Liz-Marzán, L. M.; Kostarelos, K. *In Vivo* Formation of Protein Corona on Gold Nanoparticles. The Effect of Their Size and Shape. *Nanoscale* **2018**, *10*, 1256–1264.

(10) Hadjidemetriou, M.; McAdam, S.; Garner, G.; Thackeray, C.; Knight, D.; Smith, D.; Al-Ahmady, Z.; Mazza, M.; Rogan, J.; Clamp, A.; Kostarelos, K. The Human *in Vivo* Biomolecule Corona onto PEGylated Liposomes: A Proof-of-Concept Clinical Study. *Adv. Mater.* **2019**, *31*, 1803335.

(11) Weiss, A. C. G.; Kelly, H. G.; Faria, M.; Besford, Q. A.; Wheatley, A. K.; Ang, C.-S.; Crampin, E. J.; Caruso, F.; Kent, S. J. Link between Low-Fouling and Stealth: A Whole Blood Biomolecular Corona and Cellular Association Analysis on Nanoengineered Particles. *ACS Nano* **2019**, *13*, 4980–4991.

(12) Giulimondi, F.; Digiacomo, L.; Pozzi, D.; Palchetti, S.; Vulpis, E.; Capriotti, A. L.; Chiozzi, R. Z.; Laganà, A.; Amenitsch, H.; Masuelli, L.; Mahmoudi, M.; Screpanti, I.; Zingoni, A.; Caracciolo, G. Interplay of Protein Corona and Immune Cells Controls Blood Residency of Liposomes. *Nat. Commun.* **2019**, *10*, 3686.

(13) Nedelkov, D.; Kiernan, U. A.; Niederkofler, E. E.; Tubbs, K. A.; Nelson, R. W. Investigating Diversity in Human Plasma Proteins. *Proc. Natl. Acad. Sci. U. S. A.* **2005**, *102*, 10852–10857.

(14) Corbo, C.; Molinaro, R.; Tabatabaei, M.; Farokhzad, O. C.; Mahmoudi, M. Personalized Protein Corona on Nanoparticles and Its Clinical Implications. *Biomater. Sci.* **2017**, *5*, 378–387.

(15) Hajipour, M. J.; Raheb, J.; Akhavan, O.; Arjmand, S.; Mashinchian, O.; Rahman, M.; Abdolahad, M.; Serpooshan, V.; Laurent, S.; Mahmoudi, M. Personalized Disease-Specific Protein Corona Influences the Therapeutic Impact of Graphene Oxide. *Nanoscale* **2015**, *7*, 8978–8994.

(16) Ren, J.; Cai, R.; Wang, J.; Daniyal, M.; Baimanov, D.; Liu, Y.; Yin, D.; Liu, Y.; Miao, Q.; Zhao, Y.; Chen, C. Precision Nanomedicine Development Based on Specific Opsonization of Human Cancer Patient-Personalized Protein Coronas. *Nano Lett.* **2019**, *19*, 4692–4701.
(17) Papi, M.; Caracciolo, G. Principal Component Analysis of Personalized Biomolecular Corona Data for Early Disease Detection. *Nano Today* **2018**, *21*, 14–17.
(18) Hadjidemetriou, M.; Papafilippou, L.; Unwin, R. D.; Rogan, J.; Clamp, A.; Kostarelos, K. Nano-Scavengers for Blood Biomarker Discovery in Ovarian Carcinoma. *Nano Today* **2020**, *34*, 100901.
(19) Papafilippou, L.; Claxton, A.; Dark, P.; Kostarelos, K.; Hadjidemetriou, M. Protein Corona Fingerprinting to Differentiate Sepsis from Non-Infectious Systemic Inflammation. *Nanoscale* **2020**, *12*, 10240–10253.
(20) Hajipour, M. J.; Laurent, S.; Aghaie, A.; Rezaee, F.; Mahmoudi, M. Personalized Protein Coronas: A "Key" Factor at the Nanobiointerface. *Biomater. Sci.* **2014**, *2*, 1210–1221.
(21) Caracciolo, G.; Caputo, D.; Pozzi, D.; Colapicchioni, V.; Coppola, R. Size and Charge of Nanoparticles Following Incubation with Human Plasma of Healthy and Pancreatic Cancer Patients. *Colloids Surf., B* **2014**, *123*, 673–678.
(22) Ferguson, P. R. Clinical Trials and Healthy Volunteers. *Med. Law Rev.* **2008**, *16*, 23–51.
(23) Howard, M. D.; Jay, M.; Dziubla, T. D.; Lu, X. PEGylation of Nanocarrier Drug Delivery Systems: State of the Art. *J. Biomed. Nanotechnol.* **2008**, *4*, 133–148.
(24) Suk, J. S.; Xu, Q.; Kim, N.; Hanes, J.; Ensign, L. M. PEGylation as a Strategy for Improving Nanoparticle-Based Drug and Gene Delivery. *Adv. Drug Delivery Rev.* **2016**, *99*, 28–51.
(25) Barenholz, Y. C. Doxil®—The First FDA-Approved Nano-Drug: Lessons Learned. *J. Controlled Release* **2012**, *160*, 117–134.
(26) Cui, J.; Björnmalm, M.; Liang, K.; Xu, C.; Best, J. P.; Zhang, X.; Caruso, F. Super-Soft Hydrogel Particles with Tunable Elasticity in a Microfluidic Blood Capillary Model. *Adv. Mater.* **2014**, *26*, 7295–7299.
(27) Cui, J.; De Rose, R.; Alt, K.; Alcantara, S.; Paterson, B. M.; Liang, K.; Hu, M.; Richardson, J. J.; Yan, Y.; Jeffery, C. M.; Price, R. I.; Peter, K.; Hagemeyer, C. E.; Donnelly, P. S.; Kent, S. J.; Caruso, F. Engineering Poly(ethylene Glycol) Particles for Improved Biodistribution. *ACS Nano* **2015**, *9*, 1571–1580.
(28) Cui, J.; Björnmalm, M.; Ju, Y.; Caruso, F. Nanoengineering of Poly(ethylene Glycol) Particles for Stealth and Targeting. *Langmuir* **2018**, *34*, 10817–10827.
(29) Cui, J.; Ju, Y.; Houston, Z. H.; Glass, J. J.; Fletcher, N. L.; Alcantara, S.; Dai, Q.; Howard, C. B.; Mahler, S. M.; Wheatley, A. K.; De Rose, R.; Brannon, P. T.; Paterson, B. M.; Donnelly, P. S.; Thurecht, K. J.; Caruso, F.; Kent, S. J. Modulating Targeting of Poly(ethylene Glycol) Particles to Tumor Cells Using Bispecific Antibodies. *Adv. Healthcare Mater.* **2019**, *8*, 1801607.
(30) Cui, J.; Alt, K.; Ju, Y.; Gunawan, S. T.; Braunger, J. A.; Wang, T.-Y.; Dai, Y.; Dai, Q.; Richardson, J. J.; Guo, J.; Björnmalm, M.; Hagemeyer, C. E.; Caruso, F. Ligand-Functionalized Poly(ethylene Glycol) Particles for Tumor Targeting and Intracellular Uptake. *Biomacromolecules* **2019**, *20*, 3592–3600.
(31) Wang, J.-G.; Zhou, H.-J.; Sun, P.-C.; Ding, D.-T.; Chen, T.-H. Hollow Carved Single-Crystal Mesoporous Silica Templated by Mesomorphous Polyelectrolyte–Surfactant Complexes. *Chem. Mater.* **2010**, *22*, 3829–3831.

(32) Zhang, K.; Xu, L.-L.; Jiang, J.-G.; Calin, N.; Lam, K.-F.; Zhang, S.-J.; Wu, H.-H.; Wu, G.-D.; Albela, B.; Bonneviot, L. Facile Large-Scale Synthesis of Monodisperse Mesoporous Silica Nanospheres with Tunable Pore Structure. *J. Am. Chem. Soc.* **2013**, *135*, 2427–2430.
(33) Betker, J. L.; Jones, D.; Childs, C. R.; Helm, K. M.; Terrell, K.; Nagel, M. A.; Anchordoquy, T. J. Nanoparticle Uptake by Circulating Leukocytes: A Major Barrier to Tumor Delivery. *J. Controlled Release* **2018**, *286*, 85–93.
(34) Dai, Q.; Bertleff-Zieschang, N.; Braunger, J. A.; Björnmalm, M.; Cortez-Jugo, C.; Caruso, F. Particle Targeting in Complex Biological Media. *Adv. Healthcare Mater.* **2018**, *7*, 1700575.
(35) Glass, J. J.; Chen, L.; Alcantara, S.; Crampin, E. J.; Thurecht, K. J.; De Rose, R.; Kent, S. J. Charge Has a Marked Influence on Hyperbranched Polymer Nanoparticle Association in Whole Human Blood. *ACS Macro Lett.* **2017**, *6*, 586–592.
(36) Faria, M.; Noi, K. F.; Dai, Q.; Björnmalm, M.; Johnston, S. T.; Kempe, K.; Caruso, F.; Crampin, E. J. Revisiting Cell–Particle Association *in Vitro*: A Quantitative Method to Compare Particle Performance. *J. Controlled Release* **2019**, *307*, 355–367.
(37) Schöttler, S.; Becker, G.; Winzen, S.; Steinbach, T.; Mohr, K.; Landfester, K.; Mailänder, V.; Wurm, F. R. Protein Adsorption Is Required for Stealth Effect of Poly(ethylene Glycol)- and Poly(phosphoester)-Coated Nanocarriers. *Nat. Nanotecnol.* **2016**, *11*, 372–377.
(38) Fleischer, C. C.; Payne, C. K. Secondary Structure of Corona Proteins Determines the Cell Surface Receptors Used by Nanoparticles. *J. Phys. Chem. B* **2014**, *118*, 14017–14026.
(39) Cox, J.; Hein, M. Y.; Luber, C. A.; Paron, I.; Nagaraj, N.; Mann, M. Accurate Proteome-Wide Label-Free Quantification by Delayed Normalization and Maximal Peptide Ratio Extraction, Termed MaxLFQ. *Mol. Cell. Proteomics* **2014**, *13*, 2513–2526.
(40) Vu, V. P.; Gifford, G. B.; Chen, F.; Benasutti, H.; Wang, G.; Groman, E. V.; Scheinman, R.; Saba, L.; Moghimi, S. M.; Simberg, D. Immunoglobulin Deposition on Biomolecule Corona Determines Complement Opsonization Efficiency of Preclinical and Clinical Nanoparticles. *Nat. Nanotechnol.* **2019**, *14*, 260–268.
(41) Gustafson, H. H.; Holt-Casper, D.; Grainger, D. W.; Ghandehari, H. Nanoparticle Uptake: The Phagocyte Problem. *Nano Today* **2015**, *10*, 487–510.
(42) Bertrand, N.; Grenier, P.; Mahmoudi, M.; Lima, E. M.; Appel, E. A.; Dormont, F.; Lim, J.-M.; Karnik, R.; Langer, R.; Farokhzad, O. C. Mechanistic Understanding of *in Vivo* Protein Corona Formation on Polymeric Nanoparticles and Impact on Pharmacokinetics. *Nat. Commun.* **2017**, *8*, 777.
(43) Ritz, S.; Schöttler, S.; Kotman, N.; Baier, G.; Musyanovych, A.; Kuharev, J.; Landfester, K.; Schild, H.; Jahn, O.; Tenzer, S.; Mailänder, V. Protein Corona of Nanoparticles: Distinct Proteins Regulate the Cellular Uptake. *Biomacromolecules* **2015**, *16*, 1311–1321.
(44) Horns, F.; Vollmers, C.; Dekker, C. L.; Quake, S. R. Signatures of Selection in the Human Antibody Repertoire: Selective Sweeps, Competing Subclones, and Neutral Drift. *Proc. Natl. Aca. Sci. U. S. A.* **2019**, *116*, 1261–1266.
(45) Adriani, K. S.; Brouwer, M. C.; Geldhoff, M.; Baas, F.; Zwinderman, A. H.; Morgan, B. P.; Harris, C. L.; van der Ende, A.; van de Beek, D. Common Polymorphisms in the Complement System and Susceptibility to Bacterial Meningitis. *J. Infect.* **2013**, *66*, 255–262.
(46) Tojo, T.; Friou, G.; Spiegelberg, H. Immunoglobulin G Subclass of Human Antinuclear Antibodies. *Clin. Exp. Immunol.* **1970**, *6*, 145–151.

(47) Dagley, L. F.; Infusini, G.; Larsen, R. H.; Sandow, J. J.; Webb, A. I. Universal Solid-Phase Protein Preparation (USP^3) for Bottom-up and Top-down Proteomics. *J. Proteome Res.* **2019**, *18*, 2915–2924.
(48) Rappsilber, J.; Mann, M.; Ishihama, Y. Protocol for Micro-Purification, Enrichment, Pre-Fractionation and Storage of Peptides for Proteomics Using StageTips. *Nat. Protoc.* **2007**, *2*, 1896–1906.
(49) Cox, J.; Neuhauser, N.; Michalski, A.; Scheltema, R. A.; Olsen, J. V.; Mann, M. Andromeda: A Peptide Search Engine Integrated into the MaxQuant Environment. *J. Proteome Res.* **2011**, *10*, 1794–1805.
(50) Rautela, J.; Dagley, L. F.; de Oliveira, C. C.; Schuster, I. S.; Hediyeh-Zadeh, S.; Delconte, R. B.; Cursons, J.; Hennessy, R.; Hutchinson, D. S.; Harrison, C.; Kita, B.; Vivier, E.; Webb, A. I.; Degli-Esposti, M. A.; Davis, M. J.; Huntington, N. D.; Souza-Fonseca-Guimaraes, F. Therapeutic Blockade of Activin-A Improves NK Cell Function and Antitumor Immunity. *Sci. Signaling* **2019**, *12*, eaat7527.
(51) Shah, A. D.; Goode, R. J. A.; Huang, C.; Powell, D. R.; Schittenhelm, R. B. LFQ-Analyst: An Easy-to-Use Interactive Web Platform to Analyze and Visualize Label-Free Proteomics Data Preprocessed with MaxQuant. *J. Proteome Res.* **2020**, *19*, 204–211.
(52) Babicki, S.; Arndt, D.; Marcu, A.; Liang, Y.; Grant, J. R.; Maciejewski, A.; Wishart, D. S. Heatmapper: Web-Enabled Heat Mapping for All. *Nucleic Acids Res.* **2016**, *44*, W147–W153.
(53) Faria, M.; Björnmalm, M.; Thurecht, K. J.; Kent, S. J.; Parton, R. G.; Kavallaris, M.; Johnston, A. P. R.; Gooding, J. J.; Corrie, S. R.; Boyd, B. J.; Thordarson, P.; Whittaker, A. K.; Stevens, M. M.; Prestidge, C. A.; Porter, C. J. H.; Parak, W. J.; Davis, T. P.; Crampin, E. J.; Caruso, F. Minimum Information Reporting in Bio–Nano Experimental Literature. *Nat. Nanotechnol.* **2018**, *13*, 777–785.

Table of Contents graphic